Journal of Materials Chemistry A

Accepted Manuscript

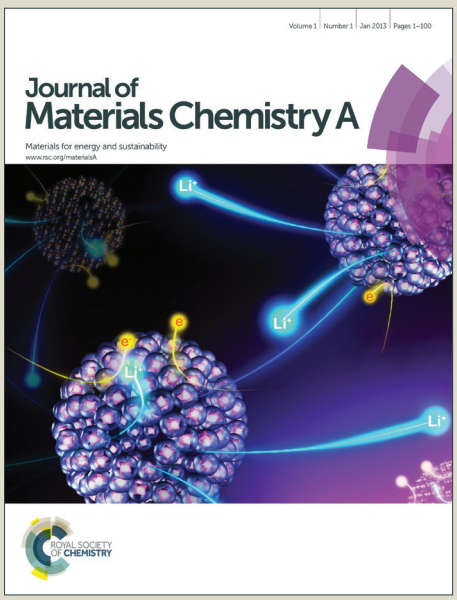

ROYAL SOCIETY OF CHEMISTRY

www.rsc.org/materialsA

Journal Name

ARTICLE

Received 00th January 20xx,
Accepted 00th January 20xx

DOI: 10.1039/x0xx00000x

www.rsc.org/

Interface Engineering for High-Performance Perovskite Hybrid Solar Cells

Zhongmin Zhou,[a] Shuping Pang,*[a] Zhihong Liu,[a] Hongxia Xu,[a] Guanglei Cui*[a]

Recently, organometal halide perovskite solar cells (PSCs) have attracted considerable attention for its extremely high power conversion efficiency (PCE). Not only does the performance of PSCs depend on the material properties of the device involved, but it is also dramatically affected by the nature of their interfaces present, which highly affect the carriers' extraction, transport and recombination. Therefore, interface engineering, a novel approach towards high-performance PSCs, has attracted increasing interests. In this review, we focus on recent advances in the study of PSCs interfaces, which have resulted in improved device performance.

Introduction

Energy shortage is one of the major challenges facing the 21st century. Currently the majority of energy sources are produced from fossil fuels, which lead to severe environmental pollution, such as fog and haze. Accordingly, searching for clean and environmentally friendly energy sources is of exceptional importance. Of the available renewable and clean energy sources, solar energy is the most abundant. Therefore, harnessing solar energy efficiently is a good solution for addressing the energy problem.

In the past decades, photovoltaic technology that directly converts sun light energy into electric energy on basis of photovoltaic effect has attracted tremendous research attention. Substantial effort has been focusing on the seeking for promising candidates to improve PCE and considerable progress has been made from organic bulk heterojunction solar cells, quantum dot solar cells, thin-film solar cells to dye-sensitized solar cells. Recently, by virtue of their appropriate and direct band gap, small exciton binding energy, well-balanced ambipolar charge transport property, earth-abundant organolead halide perovskites are considered outstanding candidates for application in solution-processed, low cost, highly efficient photovoltaic devices.[1,2]

The general chemical formula of perovskite absorber materials is AMX_3, where A is a large organic cation (typically $CH_3NH_3^+$, $HC(NH_2)_2^+$), M is a divalent metal cation (typically Pb^{2+}, Sn^{2+}), while the X anions are halides (Cl^-, Br^-, I^-). The ideal cubic crystal structure of perovskite has the M cation in 6-fold coordination, surrounded by an octahedron of anions (MX_6), and the A cation in 12-fold cuboctahedral coordination. It is interesting to note that methylammonium (MA = $CH_3NH_3^+$)-based halide perovskite materials (Fig. 1) go through structural phase transitions with temperature, with the molecular motion of the MA along the C–N axis and/or in regard to the crystal axis.[3]

In 2009, Miyasaka and co-workers reported the first lead halide perovskite sensitized solar cells with a modest PCE of 3.8%.[4] However, these cells were unstable due to the using of iodide/triiodide redox liquid electrolyte. In 2012, Park and Grätzel et al. developed solid-state mesoscopic heterojunction PSCs by employing the spiro-MeOTAD(99%) as hole transport material (HTM) yielding a PCE of 9.7%.[5] Snaith et al. reported a meso-superstructured solar cell, based on a highly crystalline perovskite ($CH_3NH_3PbI_{3-x}Cl_x$) absorber, that has a PCE of 10.9%.[6] Soak et al. combined the formamidinium lead iodide ($FAPbI_3$) with methylammonium lead bromide ($MAPbBr_3$) as the light-harvesting unit in a bilayer solar-cell architecture, and obtained a certified PCE of 17.9%.[7] Presently, a certified efficiency of 20.1% perovskite-based solar cells has been obtained, demonstrating the feasibility of these materials for highly efficient solar cells.[8]

To date, there are various film deposition methods for the fabrication of PSCs: one-step precursor solution deposition,[5] two-step sequential deposition,[9] dual-source vapor deposition and vapor-assisted solution process,[10,11] two-step spin-coating in situ intercalation,[12] anti-solvent post-treatment,[13] solvent-solvent extraction (SSE),[14] drop-casting,[15] slot-die casting[16] and gas-assisted post-treatment.[17] A perovskite solar cell is typically composed of a transparent electrode, a metal electrode, a light harvesting perovskite layer sandwiched between HTM and electron transport material (ETM). There are a variety of structures in PSCs including mesoscopic nanostructured (TiO_2, Al_2O_3, et. al) solar cells,[5,6] planar heterojunction (p-i-n and n-i-p) solar cells,[18-20] HTM-free and ETM-free solar cells as shown in Fig. 1.[15,21-23] In Table 1, part of reported performances are summarized in terms of cell components.

[a]Qingdao Key Lab of Solar Energy Utilization and Energy Storage Technology, Qingdao Institute of Bioenergy and BioprocessTechnology, Chinese Academy of Sciences, Qingdao, People's Republic of China
E-mail: pangsp@qibebt.ac.cn; cuigl@qibebt.ac.cn

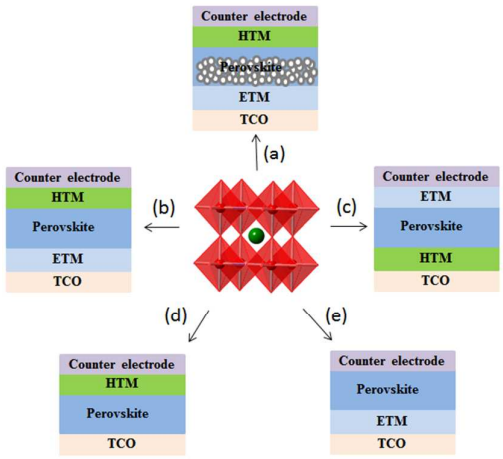

Fig. 1 Perovskite crystal structure (center) and cells structures. (a) mesoscopic nanostructured (TiO_2, Al_2O_3, et. al) PSCs. (b) planar (n-i-p) PSCs. (c) planar (p-i-n) PSCs. (d) HTM-free PSCs. (e) ETM-free PSCs.

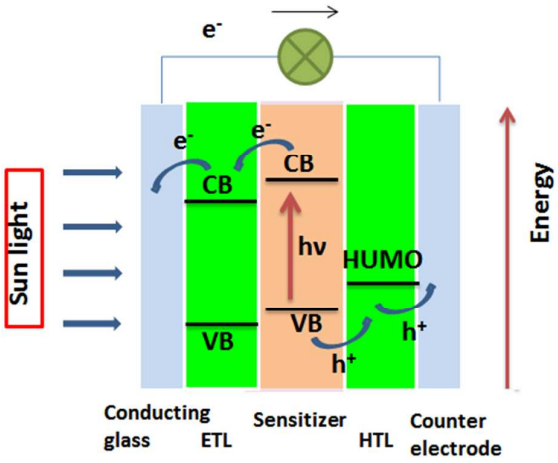

Fig. 2 Scheme of the operational principle of a $CH_3NH_3PbI_3$ perovskite sensitized solar cells.

Table 1. Photovoltaic performance of pervoskite solar cells.

Perovskite	ETM[a]	HTM[b]	J_{sc}[c] [mA/cm^2]	V_{oc}[d] [V]	FF[e] [%]	PCE[f] [%]	Ref.
$MAPbI_3$	m-TiO_2[g]	I^-/I^{-3}	11.0	0.61	57	3.81	4
$MAPbI_3$	m-TiO_2	I^-/I^{-3}	15.82	0.706	58.6	6.54	24
$MAPbI_3$	m-TiO_2	spiro-OMeTAD[h]	17.6	0.888	62	9.7	5
$MAPbI_3$	m-TiO_2	spiro-OMeTAD	10.2	0.664	48.7	3.3	25
$MAPbI_3$	C_{60}	no	13.6	0.8	50	5.4	26
$MAPbI_3$	c-TiO_2[i]	no	16.1	0.632	57	5.5	22
$MAPbI_3$	m-TiO_2/m-ZrO_2/m-Carbon	no	12.4	0.878	61	6.64	21
$MAPbI_3$	PCBM[j]	PEDOT:PSS	14.3	1.04	47	7.0	27
$MAPbI_3$	PCBM	PEDOT:PSS	10.8	0.91	76	7.41	28
$MAPbI_3$	m-TiO_2	no	18.8	0.712	60	8.0	29
$MAPbI_3$	PCBM	NiO	16.27	0.882	63.5	9.11	30
$MAPbI_3$	PCBM	PEDOT:PSS	16.1	0.84	68	9.2	31
$MAPbI_3$	PCBM	PEDOT:PSS	14.08	0.88	80.11	9.93	32
$MAPbI_3$	m-TiO_2	spiro-OMeTAD	17.06	0.937	63.5	10.15	33
$MAPbI_3$	m-TiO_2	spiro-OMeTAD	17.7	0.94	61	10.2	34
$MAPbI_3$	m-TiO_2	spiro-OMeTAD	18.3	0.865	66	10.4	35
$MAPbI_3$	m-TiO_2	spiro-OMeTAD	16.0	0.948	69	10.47	36
$MAPbI_3$	m-TiO_2	no	17.8	0.905	65	10.5	37
$MAPbI_3$	m-ZrO_2	spiro-OMeTAD	17.3	1.07	59	10.8	38
$MAPbI_3$	C-TiO_2	spiro-OMeTAD	19.1	0.92	62	10.8	39
$MAPbI_3$	m-TiO_2	no	19.0	0.84	68	10.85	40
$MAPbI_3$	m-TiO_2	spiro-OMeTAD	17.64	0.9694	67	11.5	41
$MAPbI_3$	SOHEL[k]	PEDOT:PSS	16.7	0.982	70.5	11.7	42
$MAPbI_3$	m-TiO_2	spiro-OMeTAD	16.8	1.0	71	11.9	43
$MAPbI_3$	m-TiO_2	PTAA[l]	16.5	0.997	72.7	12.0	44
$MAPbI_3$	c-TiO_2	spiro-OMeTAD	18.05	0.959	69.32	12.0	45
$MAPbI_3$	PCBM	PEDOT:PSS	16.12	1.05	67	12.0	18
$MAPbI_3$	c-TiO_2	spiro-OMeTAD	20.14	0.993	0.602	12.04	46
$MAPbI_3$	c-TiO_2	spiro-OMeTAD	19.8	0.924	66.3	12.1	11
$MAPbI_3$	PCBM/C_{60}	PEDOT:PSS	15.7	0.97	80.1	12.2	47
$MAPbI_3$	ZnO/PCBM	PTB7-Th[m]	18.18	1	67	12.2	48
$MAPbI_3$	m-TiO_2	CuSCN	19.7	1.016	62	12.4	49
$MAPbI_3$	PCBM	PEDOT:PSS	18.5	1.08	64	12.8	50
$MAPbI_3$	m-TiO_2	spiro-OMeTAD	17.9	1.036	68	12.8	51
$MAPbI_3$	PCBM	NiO/m-Al_2O_3	17.989	1.036	72.4	13.49	52

$MAPbI_3$	c-TiO_2	spiro-OMeTAD	20.71	1.02	64	13.5	53
$MAPbI_3$	m-TiO_2	OMeTPA-TPA	20.98	0.972	67	13.63	54
$MAPbI_3$	m-TiO_2	spiro-OMeTAD	19.8	1.05	64	13.7	55
$MAPbI_3$	C-TiO_2	spiro-OMeTAD	21	0.98	68	13.9	13
$MAPbI_3$	PCBM	PEDOT:PSS	20.7	0.866	78.3	14.1	56
$MAPbI_3$	m-TiO_2	spiro-OMeTAD	20.0	0.993	73	15.0	9
$MAPbI_3$	no	spiro-OMeTAD	19.9	1.07	71	15.1	57
$MAPbI_3$	PCBM/C_{60}	(Cu)-doped:NiO*x*	18.75	1.11	72	15.4	58
$MAPbI_3$	ZnO	spiro-OMeTAD	22.51	1.07	65	15.67	59
$MAPbI_3$	ZnO	spiro-OMeTAD	20.4	1.03	74.9	15.7	60
$MAPbI_3$	c-TiO_2	spiro-OMeTAD	23.38	1.06	67	15.7	61
$MAPbI_3$	c-TiO_2	spiro-OMeTAD	22	1.05	74	16.97	62
$MAPbI_3$	m-TiO_2	spiro-OMeTAD	21.64	1.056	74.1	17.01	63
$MAPbI_3$	PCBM	PEDOT:PSS	20.9	1.1	79	18.1	64
$MAPbI_{3-x}Cl_x$	c-TiO_2	spiro-OMeTAD	19.7	0.96	45	8.3	65
$MAPbI_{3-x}Cl_x$	PCBM/TiOx	PEDOT:PSS	16	0.9	66	9.8	66
$MAPbI_2Cl$	c-TiO_2	P3HT[n]	21.3	0.932	54.4	10.8	67
$MAPbI_{3-x}Cl_x$	m-TiO_2	spiro-OMeTAD	18.2	1.00	59	10.8	34
$MAPbI_{3-x}Cl_x$	c-TiO_2	spiro-OMeTAD	17.8	0.98	63	10.9	6
$MAPbI_{3-x}Cl_x$	c-TiO_2	spiro-OMeTAD	20.3	0.89	64	11.4	20
$MAPbI_{3-x}Cl_x$	PCBM	PEDOT:PSS	18.5	0.87	72	11.5	68
$MAPbI_{3-x}Cl_x$	PCBM/ C_{60}	PEDOT:PSS	18.3	0.91	70	11.65	69
$MAPbI_{3-x}Cl_x$	Fullerene/m-TiO_2	spiro-OMeTAD	19.6	0.84	72	11.7	70
$MAPbI_{3-x}Cl_x$	c-TiO_2	spiro-OMeTAD	18.0	1.02	67	12.3	71
$MAPbI_{3-x}Cl_x$	m-TiO_2	spiro-OMeTAD	19.91	1.09	65	14.15	72
$MAPbI_{3-x}Cl_x$	PCBM	PEDOT:PSS	20.61	1.0	72.5	15.0	73
$MAPbI_{3-x}Cl_x$	c-TiO_2	spiro-OMeTAD	21.7	0.97	72	15.2	74
$MAPbI_{3-x}Cl_x$	c-TiO_2	spiro-OMeTAD	21.3	1.02	68	15.3	75
$MAPbI_{3-x}Cl_x$	c-TiO_2	spiro-OMeTAD	21.5	1.07	68	15.4	10
$MAPbI_{3-x}Cl_x$	C_{60}	PEDOT:PSS	20.9	1.02	72.2	15.4	76
$MAPbI_{3-x}Cl_x$	Graphene/TiO_2	spiro-OMeTAD	21.9	1.04	73	15.6	77
$MAPbI_{3-x}Cl_x$	c-TiO_2	spiro-OMeTAD	21.5	1.02	71	15.9	78
$MAPbI_{3-x}Cl_x$	c-TiO_2	spiro-OMeTAD	24.1	1.05	72	16.5	75
$MAPbI_{3-x}Cl_x$	c-TiO_2	spiro-OMeTAD	21.7	1.04	75	16.8	79
$MAPbI_{3-x}Cl_x$	c-TiO_2	spiro-OMeTAD	22.1	1.04	75	17.3	80
$MAPbI_{3-x}Cl_x$	PCBM	PEDOT:PSS	-	-	-	18	81
$MAPbI_{3-x}Cl_x$	Yttrium-TiO_2	spiro-OMeTAD	22.75	1.13	75.01	19.3	82
$MAPbBr_3$	c-TiO_2	PDI[o]	1.08	1.30	40	0.56	83
$MAPbBr_3$	m-TiO_2	PCBTDPP[p]	4.47	1.16	59	3.04	84
$MAPbBr_3$	m-TiO_2	Br^-/Br^{-3}	5.57	0.96	59	3.13	4
$MAPbBr_3$	m-TiO_2	PTAA	5.0	1.13	74	4	85
$MAPbBr_3$	m-TiO_2	PTAA	6.1	1.40	79	6.7	86
$MAPbBr_3$	c-TiO_2	PIF8-TAA[q]	8.4	1.51	82	10.4	87
MAPbIBr2	c-TiO_2	no	16.2	0.77	68	8.54	88
$MAPb(I_{1-x}Br_x)_3$	m-TiO_2	PTAA	18.0	0.87	66	12.3	89
$MAPb(I_{1-x}Br_x)_3$	m-TiO_2	PTAA	19.58	1.105	76	16.2	90
$MAPbBr_{3-x}Cl_x$	c-TiO_2	CBP[r]	4.0	1.50	46	2.7	91
$MAPbBr_{3-x}Cl_x$	c-TiO_2	CBP	7.8	1.24	56	5.4	92
$FAPbI_3$	m-TiO_2	P3HT	18.3	0.84	50	7.5	93
$FAPbI_3$	c-TiO_2	spiro-OMeTAD	23.3	0.94	65	14.2	94
$FAPbI_3$	m-TiO_2	spiro-OMeTAD	20.97	1.032	74	16.01	95
$FAPbI_3$	PCBM	NiO	24.7	1.06	77.5	20.2	96
$FAPbI_{3-x}Cl_x$	m-TiO_2	P3HT	19.24	0.73	54	7.51	97
$FAPbBr_3$	c-TiO_2	spiro-OMeTAD	6.6	1.35	73	6.5	98
$FA_{0.4}/MA_{0.6}PbI_3$	m-TiO_2	spiro-OMeTAD	21.2	1.003	70	14.9	99
$(FAPbI_3)_{0.85}$ $(MAPbBr_3)_{0.15}$	m-TiO_2	PTAA	22.5	1.11	73.2	17.9	7
$MASnBr_3$	m-TiO_2	spiro-OMeTAD	7.93	0.88	59	4.27	100
$MASnI_3$	m-TiO_2	spiro-OMeTAD	16.6	0.68	48	5.23	100
$MASnI_2Br$	m-TiO_2	spiro-OMeTAD	13.96	0.77	50	5.48	100
$MASnIBr_2$	m-TiO_2	spiro-OMeTAD	11.73	0.82	57	5.73	100
$MASn_{0.5}Pb_{0.5}I_3$	m-TiO_2	P3HT	20.04	0.42	50	4.18	101
$MAPb_{1-a}Sn_aI_{3-x}Cl_x$	PCBM	PEDOT:PSS	19.1	0.76	66	9.77	102

a. ETM: electron transporting materials; b. HTM: hole transporting layers; c. J_{SC}: short-circuit current; d. V_{OC}: open-circuit voltage; e. FF: fill factor; f. PCE: power conversion efficiency; g. m-TiO_2: Mesoporous TiO_2; h. spiro-OMeTAD: 2,2',7,7'-tetrakis (N,N'-di-p-methoxyphenyl-

amine)-9,9′-spirobifluorene(spiro-OMeTAD); i. c-TiO_2: compact TiO_2; j. PCBM: phenyl -C_{61}-butyric acid methyl ester; k. SOHEL: tetrafluoroethylene-perfluoro-3,6-dioxa-4-methyl -7-octene-sulfonic acid copolyme;. l. PTAA: poly(triarylamine); m. PTB7-Th: poly[4,8-bis(5-(2-ethylhexyl)thiophen-2-yl)benzo [1,2-b:4,5-b']dithiophene-co-3–fluorothieno [3,4-b]thiophene-2-carboxylate]; n. P3HT: poly(3-hexylthiophene-2,5-diyl); o. PDI: perylene-diimide; p. PCBTDPP: poly[N-9-hepta-decanyl-2,7-carbazole-alt-3,6-bis-(thiophen-5-yl)-2,5-dioctyl-2,5-dihydropyrrolo [3,4-]pyrrole-1,4-dione]; q. PIF8-TAA: poly-indenofluoren-8-triarylamine; r. CBP: 4,4′-bis (N-carbazolyl)-1,1′-biphenyl.

Fig. 2 schematically shows the work mechanism of a solid state PSCs. The cell's working principle involves the following processes: the perovskite material produces the carriers (electron and hole) after absorbing light. The electron is separated from the hole, then is injected into ETM and migrates to the anode. Subsequently, the electron passes through the external circuit to the cathode. At the same time, the hole transfers into HTM, then migrates to the cathode, at which they encounter and recombine. Carriers extraction and injection occur at the perovskite/electron transport layer (ETL) or hole transport layer (HTL) interfaces and the ETL or HTL/electrode layer interfaces, respectively. Therefore, the properties of these interfaces influence the device performance dramatically. Similarly when it goes to a cell, not only does the performance of solar cells depend on the molecular properties of the cell components involved, but it is also dramatically affected by the nature of the interfaces present. As a matter of fact, it is well recognized that interface modification is an efficient way to achieve high-performance solar cells, since it can improve open-circuit voltage and eliminate the photocurrent hysteresis, etc.[47,103] Therefore, interface engineering has become an significant approach to fabricate high-performance PSCs. Recently, there are many reports that focused on the modification of the device interfaces, such as ETL/metal electrode interfaces,[47,52,56,73,104-107] ETL/perovskite interfaces,[33,48,59,80,82,108-112] and ETL/transparent electrode (ITO) interfaces.[57,82] It is said that HTL/perovskite interfaces have an important influence on device performance.[61,75,113] In addtion, modification of perovskite/metal electrode interfaces can lead to a higher PCE.[114]

Despite some progress in the investigation of interfaces, a deeper understanding of interface phenomena and exploration of novel interface modification techniques are still required for the sake of improving the overall performance. In this review, we limit ourselves to summarize recent progress of the materials and technologies associated with interfacial engineering instead of focusing on interfacial theory and charge dynamics for PSCs, which were recently reviewed elsewhere.[115] We hope that interfacial engineering of PSCs attracts more attention in order to promote the development of this type of solar cells.

Energy level Alignment at the Interfaces

Energy level alignment at the interfaces, to a great extent, affecting device parameters, is critical for optimization of the device.[116,117] Proper matching of the electronic energy level of adjacent layers is necessary to obtain high power conversion efficiency. Only if electrons are extracted from the perovskite into the lowest unoccupied molecular orbital (LUMO) of the ETL while holes are transferred to the highest occupied molecular orbital (HOMO) of the HTL that device can operate efficiently.[118] The ETL (also called hole-blocking layer) is needed to prevent holes formed in the perovskite layer from reaching the cathode,

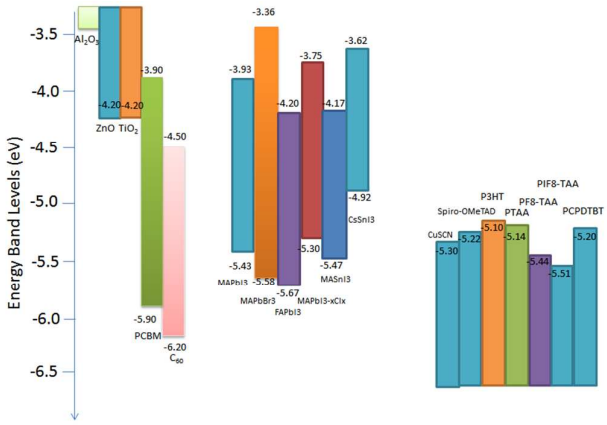

Fig. 3. Schematic energy level diagram of different materials in solar cells. MA and FA stand for methylammonium (CH_3NH_3) and formamidinium ($HC(NH_2)_2$), respectively.

as this would short-circuit the cell.[119] The band offset between ETL/perovskite is a key factor for carriers recombination at the interface. Suitable offset (~0.2 eV) can ensure the efficient injection of electrons from perovskite to the ETL.[120] When the LUMO of the ETL is too lower than that of the perovskite, the V_{oc} will decrease, while a much smaller offset will induce remarkable carriers recombination. Similarly, the HOMO of the HTM should be a little higher than that of the perovskite to efficiently extracting the holes and blocking the electrons. In addition, the two electrodes should facilitate better charge transfer from the adjacent layers and their workfunctions should match the energy levels of the adjacent layers. The energy levels for the commonly used materials in PSCs are shown in Fig. 3. Rationalizations of the function and performance of PSCs have been based mostly on device energy diagrams derived from energy values of the isolated components.[121] It is worth mentioning that mismatching energy levels between adjacent layers can be adjusted through surface modification.[122]

ETL/Perovskite Interface

Improvement of Carrier Extraction and Injection

Improving the electron extraction and injection is an important approach to enhancing the efficiency of PSCs. The two major processes, electron extraction and injection, occur at the ETL/perovskite layer interface. Therefore, the properties of this interface have a key influence on the device performance. And much efforts have been devoted to the modification of the ETL/perovskite interfaces.

A fast extraction of the photo-induced carriers is necessary to enhance charge collection efficiency. The ETL/perovskite interface has a key influence on electron extraction. To ensure efficient electron extraction, a suitable ETL has to be energetically compatible with the perovskite absorber. Introduction of an additive between the ETL and perovskite layer is a common

approach for the interface modification. PCBM was introduced to modify the surface of the ETL (ZnO) in device structure of ITO/ZnO/$CH_3NH_3PbI_3$/PTB7-Th/MoO_3/Ag.[48] Ultraviolet photo-electron spectroscopy (UPS) was used to investigate the electronic structures of ZnO and ZnO/PCBM. With regard to the ZnO/PCBM ETL, the CBM of ZnO/PCBM is located between that of ZnO and that of perovskite, so much more favorable energy-level alignment occurs at the interfaces, facilitating cascade charge extraction. In addition, the V_{oc} which is usually determined by the energy-level offset between the quasi Fermi levels of the ETL and the HTL adjacent to the perovskite absorber were further enhanced relative to those of bare ZnO-based devices.[6,86]

For PSCs, faster electron injection is always desirable in competing with carrier trapping and even thermalization/cooling, because a large amount of the converted photon energy has to be wasted in above processes. Graphene quantum dots (GQDs) were introduced as an ultrathin layer between perovskite and TiO_2 (Fig. 4a), achieving a significant PCE improvement from 8.81% to 10.15%. [33] Femtosecond transient absorption (fs-TA) spectroscopy was used to investigate the role of the ultrathin GQDs layer in the device. They found that much faster electron extraction with the presence of GQDs (90 ~ 106 ps) than without their presence (260~307 ps) happened, namely, GQDs can act as an ultrathin glue to enhance the electronic coupling and as a superfast electron funnel to efficiently mediate the electron transfer from the absorber to acceptor. So it can significantly enhance the electron extraction from perovskite to TiO_2. Ogomi et al. introduced HOCO-R-$NH_3^+I^-$ between the porous TiO_2 and the perovskite layer (Fig. 4b),[108] and observed that electron injection from perovskite to TiO_2 became faster after HOCO-R-$NH_3^+I^-$ was inserted in the interface between TiO_2 and perovskite.

Suppression or Reduction of Carrier Recombination

Carrier recombination is detrimental to device performance. Weak recombination at the interfaces will bring high V_{OC} in the PSCs.[115] Therefore, suppression or reduction of carrier recombination through appropriate interfacial engineering for the perovskite-based solid hybrid solar cells is very important for achieving high efficiency.[123] Ogomi et al. found that carrier recombination could be suppressed by inserting HOCO-R-$NH_3^+I^-$ anchor group between ETL/perovskite layer.[108] They investigated the charge recombination dynamics between electrons in TiO_2 and holes in perovskite by using nanosecond using transient absorption (ns-TA) spectroscopy. For perovskite/TiO_2 without HOCO-R-$NH_3^+I^-$, no TA signal could be observed. This indicated that the recombination time between electrons injected into TiO_2 and holes in perovskite was less than 1 μs (the TA signal appeared is typically longer than μs in the time scale). For perovskite/TiO_2 with HOCO-R-$NH_3^+I^-$, however, a TA signal could be observed clearly, which disappeared in around 10 μs. This result suggested that the as-inserted HOCO-R-$NH_3^+I^-$ between TiO_2 and perovskite could greatly suppress recombination of the electrons in TiO_2 and holes in perovskite. So the introduction of HOCO-R-$NH_3^+I^-$ can enhance the device performance.

Impedance spectroscopy (IS) can be used to investigate the charge recombination processes by extracting the recombination resistance (R_{rec}) from its measurements in PSCs. Charge recombination processes can be revealed by the features observed in the low-frequency region in the IS spectra, and the R_{rec} can be obtained by fitting the Nyquist plots in this region.[124] Taking Lee and his co-workers' work as an example, they obtained the R_{rec} values of the PSCs with ZnO and ZnO/PCBM at different applied voltages under 1-sun illumination (Fig. 4c).[48] The cell with ZnO/PCBM showed higher R_{rec} values (lower recombination rate) than those of the device with only ZnO at low applied bias, suggesting that the interfacial modification could suppress the surface charge recombination greatly.[125] They also found that bulk charge recombination, which corresponded to the higher R_{rec} values obtained at high applied bias, could be decreased by the interfacial modication of ZnO.[109]

Han et al. introduced an organic silane self-assembled monolayer (SAM) in device structure of FTO/TiO_2/ZrO_2/$H_3NH_3PbI_3$/Carbon to modify the interface between ETL and perovskite.[110] The introduction of the silane SAM can achieve a larger built-in potential, which contribute to the separation of photogenerated carriers and the suppression of electrons from TiO_2 to $CH_3NH_3PbI_3$. At the same time, the device with the silane SAM obtained a longer charge-carrier lifetime, which is conducive to the hole transport through the perovskite/ZrO_2 layer before reaching the carbon back contact. So the silane SAM can help to suppress the carriers recombination. An effective way of controlling the charge recombination is to change the electrical properties of the wide band gap semiconductors by coating the nanoparticle surfaces. MgO was successfully introduced by being spin-coated onto the mesoporous TiO_2 layer to suppress charge recombination.[111] Transient photovoltage decay data demonstrated that recombination times for MgO-coated TiO_2 nanoparticle-based PSCs was about three times longer than those of TiO_2 nanoparticle-based device. The longer recombination time was responsible for enhancing the V_{oc} and FF of MgO-coated TiO_2 nanoparticle-based PSCs.

Apart from the mentioned above, there are some other interfacial modifications between ETL/perovskite interface layer. For example, the introduction of C_{60}-substituted benzoic acid self-

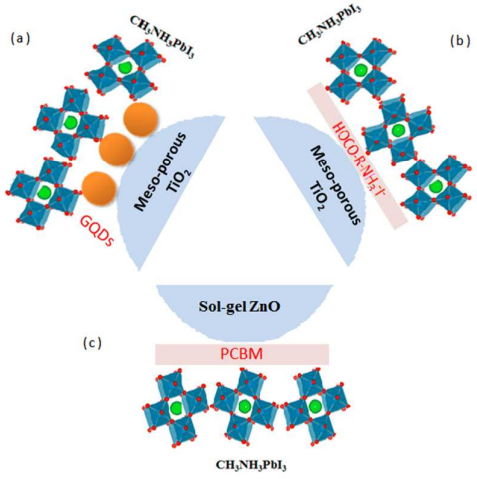

Fig. 4. Schematic diagram of (a) $CH_3NH_3PbI_3$/GQDs/TiO_2 structure; (b) $CH_3NH_3PbI_3$/HOCO-R-$NH_3^+I^-$/TiO_2 structure; (c) ZnO/PCBM/ $CH_3NH_3PbI_3$ structure.

assembled monolayer (C_{60}SAM) on the surface of both the mesoporous and compact TiO_2 can enhance the V_{oc} and FF comparison to the "bare" TiO_2-perovskite solar cells, further improving the PCE of the device.[80,109] Li et al. introduced 3-aminopropanoic acid SAM (C3-SAM) between the sol-gel ZnO and perovskite layers.[59] It lead to significant improvement both in the morphology of $CH_3NH_3PbI_3$ perovskite film and in alignment of interfacial energy level, enhancing the PCE from 11.96% to 15.67%. It is also reported that yttrium was introduced to modify TiO_2 with the aim of improving the electron transport property.[82] Additionally, the modification can also control the growth of the crystal due to the enhancement of the compatibility to the perovskite materials and contribute to the higher PCE. [108,112]

ETL/Metal Electrode Interface

The widely used inverted PSCs structure is ITO/PEDOT:PSS/ Perovskite/ETL/Metal electrode. Phenyl-C_{61}-butyric acid methyl ester (PCBM) is often used as the ETL. The ETL/metal electrode layer interface has a key influence on electron collection of the metal electrode from the ETL. Introducing proper interfacial materials to modify the interfaces of the electron transport layer and the metal electrode is an important approach to improve PSCs performances.[47,56,73] Seok and his coworkers introduced a thin LiF layer (0.5 nm) between PCBM and Al electrode in the cells.[56] The insertion of the LiF layer can contribute to a improvement both in the FF and J_{sc}, compared to those of a device without a LiF layer. In organic solar cells, the introduction of LiF had already been reported.[126,127] This modification could generate a dipole moment across the interfaces that can reduce energy barrier between PCBM/Al leading to the improvement of the electron migration from the PCBM to the LiF/Al.[56] By inserting the LiF interlayer and choosing the optimal thickness of the PCBM layer, they fabricated highly efficient devices with PCE of 14.1% (J_{sc} of 20.7 mA/cm^2, V_{oc} of 0.866 V, FF of 78.3%) under AM 1.5 G 100 mW/cm^2 irradiation.

It is also reported that an amino-functionalized polymer (PN_4N) was introduced to modify the interface between ETL and metal electrode.[73] The modified interface can reduce leakage current at the cathode, because comparing to the dark current density of the devices with bare Al cathode under reverse bias, it is about one order of magnitude smaller with PN_4N/Al bilayer cathode. In addition, it has been reported in polymer solar cells that the interfacial modification of the insertion of PN_4N can eliminate the trap states at the PCBM/metal electrode interface, leading to the reduction of the recombination of charges at the cathode interface and reduce the injection barrier between the PCBM and the metal electrode and then lead to an improvement of the electron transport in the device.[128,129] This modification resulted in a remarkable enhancement of PCE from 12.4% to 15.0%. Besides, photocurrent hysteresis was insignificant, which might be attributed to the improved cathode interface modified by PN_4N.

Zhang et al. introduced ZnO or perylene-diimide (PDINO) layers to modify the PCBM/Ag interface.[130] Both ZnO and PDINO layers can effectively modify the PCBM/Ag interface and improve the V_{oc}. A high PCE > 13% is achieved in PDINO-based devices compared with that of ZnO-based devices. PDINO plays key role, one hand, providing the desired electronic levels for electron

Table 2. Interfacial material and the corresponding ETL and Counter electrode.

ETL	Interfacial material	Counter electrode	PCE [%]	Ref.
PCBM	**LiF**	Al	14.1	56
PCBM	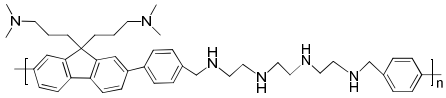 PN_4N	Al	15	73
C_{60}	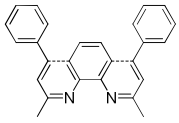 BCP	Al	12.2	47
PCBM	**BCP**	Al	7.8	104
PCBM	**BCP**	Au	6.13	105
PCBM	**ZnO** or 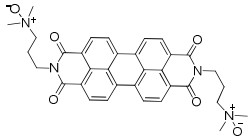 PDINO	Ag	14	133
PCBM	**BCP**	Ag	13.61	52
PCBM	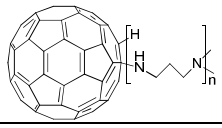	Ag	13.4	106

PCBM	DMAPA- C_{60} **Bis-C_{60}**	Ag	11.8	107

extraction, producing uniform films with favorable collection,and low series resistance, and, the other hand, successfully preventing Ag ions diffusing to the semiconductor interface during the evaporation. In addition, PDINO-based devices also show the higher stability relative to these of devices with PCBM/Ag and PCBM/ZnO/Ag cathodes.

Bathocuproine (BCP) is often used as an electron transporting or hole blocking layer in organic light emitting diodes, organic photodetectors and organic photovoltaic devices for its fabulous electron mobility and poor hole mobility.[131-133] It was also introduced as hole blocking layer between double fullerene layers and metal electrode in PSCs, besides, with the aim of reducing the damage of the fullerene layer followed by metal deposition.[47,52,104,105] There are also fullerene and its derivative that were introduced to modify the interface between ETL and Ag electrode. Both are conducive to the improvement of the device peformance.[106,107]

ETL/Transparent Conducting Oxide (ITO) Interface

The ITO can be used both in a normal architecture and an inverted structure, therefore, their roles can switch from collecting holes to electrons. The workfunction of ITO (4.6 eV) makes it possible for ITO to collect either holes or electrons depending mainly on the contact properties of the coating layer on top of the ITO surface. In the inverted structure, it is coated with a high workfunction layer (PEDOT:PSS) which collects holes. In the normal structure, it is generally coated with a compact n-type metal oxide (TiO_2) which could prevent direct contact between the ITO and HTM. As for the latter, a Schottky barrier exists at the ITO/TiO_2 interface, which may lead to adverse effect on the device.[134] However, this can be improved through modifying electron energy level matching between the ITO and the TiO_2, and more precise control over the doping level in the TiO_2. Yang et al. introduced a solution of polyethyleneimine ethoxylated (PEIE) in methoxyethanol (~0.1% by weight) forming an ultrathin layer on the ITO surface.[82] The introduced molecular dipole interactions successfully reduced the work function of ITO from 4.6 eV to 4.0 eV.

Only if achieving optimized interface energy level alignment between ITO and perovskite light absorber and preventing direct contact between the ITO and the HTM, a compact n-type metal oxide is not necessary for a normal structure. An exceptional approach to modify the ITO was reported in perovskite solar cells.[57] Cesium carbonate (Cs_2CO_3) solution was used to modify the ITO surface, as shown in Fig. 5. Cs_2CO_3 did not form a continuous compact film but discontinuous islands on the ITO surface. This modification tuned the surface work function, leading to an optimized interface energy level alignment between ITO and perovskite light absorber, accordingly, facilitating the electron collection efficiency from the perovskite layer to the ITO substrate and leading to higher device performance.

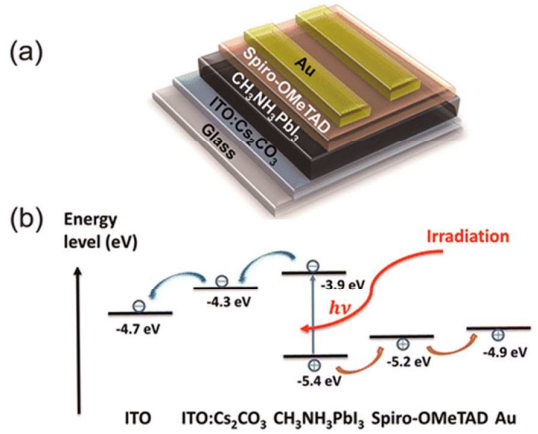

Fig. 5. Device architecture. (a) Schematic of the device structure; (b) Energy level diagram. Reprinted with permission from ref. 57.

Perovskite /HTL Interface

The function of HTL is blocking electron and transporting hole. The hole extraction, which is an important process in PSCs, occurs at the HTL/perovskite layer interface. Highly efficient hole extraction at the perovskite/HTL interface helps to improve device performance owing to a depletion of holes within the perovskite film, limiting opportunities for charge recombination.[23] Therefore, it is necessary to achieve successful electron blocking and efficient hole extraction by interface engineering between HTL and perovskite interface.[50] In addition, trap states at the perovskite surface can generate charge accumulation and lead to recombination losses in device. Meanwhile, native dipoles occurring at the organic-inorganic interface, between the HTL and the perovskite layers, would contribute to the hysteresis.[135] Thus, eliminating or reducing trap states through interface modification is conductive to device performance.

We all know that there exist hole traps on the surfaces of three dimensional (3D) $CH_3NH_3PbI_3$ perovskite thin films.[136] The hole traps resulting from the under-coordinated halide anions on the surface of perovskite crystal, will lead to a significant accumulation of charge at the perovskite/hole transporter heterojunction. Consequently, introduction of an external material to saturate the under-coordinated halide anions is an efficient approach to reduce charge recombination. Snaith et al. have done pioneering work to introduce iodopentafluorobenzene (IPFB) through supramolecular halogen bonding donor-acceptor complexation to passivate perovskite surface hole trapping states.[61] This engineering inhibited charge recombination and lead to fast and efficient charge extraction. The best PCE of the IPFB-treated devices increased from 13.0% to 15.7% (Fig. 6a).

There are under-coordinated ions at crystal surfaces and also at the grain boundaries between individual perovskite crystals. The under-coordinated Pb atoms in the perovskite crystal can be passivated via coordinate bonding between the sulfur atom in thiophene or nitrogen atom in pyridine.[75] The treatment between HTL and perovskite interface with the Lewis bases, thiophene and pyridine, can result in a significant decrease in the rate of nonradiative recombination in perovskite films and increase the

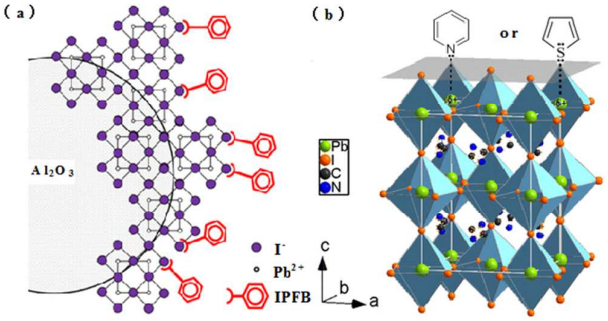

Fig. 6. (a) Proposed interaction between the IPFB and generic halogen anions; (b) Possible passivation mechanism: Pyridine or thiophene molecules can effectively neutralizing the excess positive charge in the crystal. Reprinted with permission from ref. 61 and 75.

efficiency of PSCs from 13% to 15.3% and 16.5%, respectively (Fig. 6b). The instability of PSCs mainly arises from the CH_3NH_3 group (in $CH_3NH_3PbI_3$) which is vulnerable to moisture. This can be ameliorated by changing the hydrophilic nature of the perovskite surface to a hydrophobic one. Dodecyltrimethoxysilane (C_{12}-silane) as a amphiphilic molecular comprises hydrophobic long alkyl chain and electrophilic trimethoxysilane groups, which can change into Si-OH to bond I^- in the perovskite surface.[113] The introduction of this interlayer between HTL and perovskite can make the surface of the perovskite more resistant to moisture, meanwhile, function as an electrically insulating barrier, reducing interfacial charge recombination losses in perovskite solar cells, resulting in an increase in FF and V_{oc}.

Perovskite/Metal Electrode Interface

The HTL is a very important component in the PSCs, however, there is HTL-free cell device that has been reported.[15,21-22,38] It was demonstrated that perovskite material itself can transport holes. A Schottky contact exists at the perovskite/metal electrode interface in HTM-free PSCs. Therefore it is required to develop suitable methods to modify the perovskite/metal electrode interface in order to improve the device performance.

As a wide band gap organic semiconductor, N,N,N',N'–tetraphenyl benzidine (TPB) has been widely used in OLEDs.[137] Recently, it has been introduced into PSCs.[114] The HOMO energy level of TPB (−6.0 eV) is lower than the valence band edge of $CH_3NH_3PbI_3$ (−5.4 eV). Therefore, the TPB is not suitable as the hole conductor for its mismatched band alignment in the band structure. However, the introduction of a thin TPB layer can increase the recombination resistance, which may help to reduce the dark current and lead to the improvement in V_{oc}. In other words, the TPB layer can well suppress the electron recombination at the back Schottky contact and improve the device performance.

Summary and Outlook

Great progress has been made in PSCs in the past six years. However, to realize practical applications, further efforts to improve overall device performance including high efficiency, excellent stability, low cost, and nontoxic absorber materials are still required. There is much room to improve the photovoltaic performance of the organolead halide perovskite-based solar cells by interface engineering.

Featuring a bandgap of 1.45 eV, the $FAPbI_3$ has the potential to achieve higher performance than $MAPbI_3$. The highest PCE[96] is based on $FAPbI_3$ material which are crystallized into large-grained films through the direct intramolecular exchange of dimethylsulfoxide molecules intercalated in PbI_2 with formamidinium iodide. There is scarcely any report about interfacial engineering in $FAPbI_3$-based PSCs. Therefore, it will attract increasing attention to improve $FAPbI_3$-based device performance by interfacial engineering. Moreover, the long-term stability of PSCs is a pressing, unsolved questions. The reported longest time of device stability so far is about 2000 h under temperatures of 80–85 degrees Celsius.[138] This is far from practical application. The stability of interfaces between adjacent layers is an important factor. From this point, interface engineering would be an effective approach to improve the stability of the device.

To date, most attention has been paid to the modification of the ETL/metal electrode interface and ETL/perovskite interface. Further investigations of the perovskite/HTL interface and HTL/electrode interface are still required. As has been pointed out by Johansson and coworkers, the efficiencies can be primarily determined by recombination at the perovskite/HTL interface.[139] The hole transport materials are currently the bottleneck for the realization of cost effective and stable devices. Although it was shown that without using HTL a high PCE of 10% can be achieved, the use of an additional HTM layer significantly improves the device performance. Rencently, Miyasaka et.al pointed out that the interface between FTO and TiO_2 compact Layer is one of the origins to hysteresis in planar heterojunction PSCs.[140] More efforts, therefore, need to be focus on this interface to reduce hysteresis and enhance performance.

In conclusion, with a deeper understanding of interface phenomena and exploration of novel interface modification approaches, interface engineering is expected to drive further development of PSCs. We expect that higher efficiency will be obtained after more research work on the interfaces of PSCs.

Acknowledgements

Financial support for this work from the Chinese National Natural Science Foundation (51202266, 21202178), Natural Science Foundation of Shandong Province (ZR2013FZ001), the Research Program of Qingdao (13-1-4-228-jch, 14-2-4-8-jch).

References

1. S. D. Stranks, G. E. Eperon, G. Grancini, C. Menelaou, M. J. P. Alcocer, T. Leijtens, L. M. Herz, A. Petrozza and H. J. Snaith, *Science*, 2013, **342**, 341-344.
2. G. Xing, N. Mathews, S. Sun, S. S. Lim, Y. M. Lam, M. Grätzel, S. Mhaisalkar and T. C. Sum, *Science*, 2013, **342**, 344-347.
3. H. S. Jung and N.–G. Park, *small*, 2015, **11**, 10–25.
4. A. Kojima, K. Teshima, Y. Shirai and T. Miyasaka, *J. Am. Chem. Soc.*, 2009, **131**, 6050-6051.
5. H.-S. Kim, C.-R. Lee, J.-H. Im, K.-B. Lee, T. Moehl, A. Marchioro, S.-J. Moon, R. Humphry-Baker, J.-H. Yum, J. E. Moser, M. Grätzel and N.-G. Park, *Sci. Rep.*, 2012, **2**, 591.
6. M. M. Lee, J. Teuscher, T. Miyasaka, T. N. Murakami and H.

J. Snaith, *Science*, 2012, **338**, 643-647.
7. N. J. Jeon, J. H. Noh, W. S. Yang, Y. C. Kim, S. Ryu, J. Seo and S. Il Seok, *Nature*, 2015, **517**, 476-480.
8. NREL, www.nrel.gov/ncpv/images/efficiency_chart.jpg, 2014.
9. J. Burschka, N. Pellet, S. J. Moon, R. Humphry-Baker, P. Gao, M. K. Nazeeruddin and M. Grätzel, *Nature*, 2013, **499**, 316-319.
10. M. Liu, M. B. Johnston and H. J. Snaith, *Nature*, 2013, **501**, 395-398.
11. Q. Chen, H. Zhou, Z. Hong, S. Luo, H. S. Duan, H. H. Wang, Y. Liu, G. Li and Y. Yang, *J. Am. Chem. Soc.*, 2014, **136**, 622-625.
12. S. Ahmad, P. K. Kanaujia, W. Niu, J. J. Baumberg and G. V. Prakash, *ACS Appl. Mater. Interfaces*, 2014, **6**, 10238−10247.
13. M. Xiao, F. Huang, W. Huang, Y. Dkhissi, Y. Zhu, J. Etheridge, A. Gray-Weale, U. Bach, Y.-B. Cheng and L. Spiccia, Angew. Che., Int. Ed., 2014, 53, 9898-9909.
14. Y. Zhou, M. Yang, W. Wu, A. L. Vasiliev, K. Zhu and N. P. Padture, *J. Mater. Chem. A*, 2015, **3**, 8178–8184.
15. A. Mei, X. Li, L. Liu, Z. Ku, T. Liu, Y. Rong, M. Xu, M. Hu, J. Chen, Y. Yang, M. Grätzel and H. Han, *Science*, 2014, **345**, 295-298.
16. K. Hwang, Y.-S. Jung, Y.-J. Heo, F. H. Scholes, S. E. Watkins, J. Subbiah, D. J. Jones, D.-Y. Kim and D. Vak, *Adv. Mater.*, 2015, **27**, 1241–1247.
17. Z. Zhou, Z. Wang, Y. Zhou, S. Pang, D. Wang, H. Xu, Z. Liu, N. P. Padture and G. Cui, *Angew. Chem. Int. Ed.*, 2015, **54**, DOI: 10.1002/anie.201504379.
18. O. Malinkiewicz, A. Yella, Y. H. Lee, G. M. Espallargas, M. Grätzel, M. K. Nazeeruddin and H. J. Bolink, *Nat. Photon.*, 2014, **8**, 128-132.
19. J. Y. Jeng, Y. F. Chiang, M. H. Lee, S. R. Peng, T. F. Guo, P. Chen and T. C. Wen, *Adv. Mater.*, 2013, **25**, 3727-3732.
20. G. E. Eperon, V. M. Burlakov, P. Docampo, A. Goriely and H. J. Snaith, *Adv. Funct. Mater.*, 2013, **24**, 151-157.
21. Z. Ku, Y. Rong, M. Xu, T. Liu and H. Han, *Sci. Rep.*, 2013, **3**, 3132.
22. L. Etgar, P. Gao, Z. Xue, Q. Peng, A. K. Chandiran, B. Liu, M. K. Nazeeruddin and M. Grätzel, *J. Am. Chem. Soc.*, 2012, **134**, 17396-17399.
23. D. Liu , J. Yang and T. L. Kelly, *J. Am. Chem. Soc.*, 2014, **136**, 17116-17122.
24. J. H. Im, C. R. Lee, J. W. Lee, S. W. Park and N. G. Park, *Nanoscale*, 2011, **3**, 4088-4093.
25. L. Qiu, J. Deng, X. Lu, Z. Yang and H. Peng, *Angew. Chem. Int. Ed.*, 2014, **53**, 10425-10428.
26. H. Hu, D. Wang, Y. Zhou, J. Zhang, S. Lv, S. Pang, X. Chen, Z. Liu, N. P. Padture and G. Cui, *RSC Adv.*, 2014, **4**, 28964-28967.
27. C. Roldan-Carmona, O. Malinkiewicz, A. Soriano, G. M. Espallargas, A. Garcia, P. Reinecke, T. Kroyer, M. I. Dar, M. K. Nazeeruddin and H. J. Bolink, *Energy Environ. Sci.*, 2014, **7**, 994-997.
28. S. Y. Sun, T. Salim, N. Mathews, M. Duchamp, C. Boothroyd, G. C. Xing, T. C. Sum and Y. M. Lam, *Energy Environ. Sci.*, 2014, **7**, 399-407.
29. W. A. Laban and L. Etgar, *Energy Environ. Sci.*, 2013, **6**, 3249-3253.
30. Z. Zhu, Y. Bai, T. Zhang, Z. Liu, X. Long, Z. Wei, Z. Wang, L. Zhang, J. Wang, F. Yan and S. Yang, *Angew. Chem., Int. Ed.*, 2014, **53**, 12571-12575.
31. Y. Chen, J. Peng, D. Su, X. Chen and Z. Liang, *ACS Appl. Mater. Interfaces*, 2015, **7**, 4471-4475.
32. C. Zuo and L. Ding, *Nanoscale*, 2014, **6**, 9935-9938.
33. Z. Zhu, J. Ma, Z. Wang, C. Mu, Z. Fan, L. Du, Y. Bai, L. Fan, H. Yan, D. L. Phillips and S. Yang, *J. Am. Chem. Soc.*, 2014, **136**, 3760-3763.
34. L. Zheng, Y. Ma, S. Chu, S. Wang, B. Qu, L. Xiao, Z. Chen, Q. Gong, Z. Wu and X. Hou, *Nanoscale*, 2014, **6**, 8171-8176.
35. J. H. Noh, N. J. Jeon, Y. C. Choi, M. K. Nazeeruddin, M. Grätzel and S. Il Seok, *J. Mater. Chem. A*, 2013, **1**, 11842-11847.
36. J. Shi, Y. Luo, H. Wei, J. Luo, J. Dong, S. Lv, J. Xiao, Y. Xu, L. Zhu, X. Xu, H. Wu, D. Li, and Q. Meng, *ACS Appl. Mater. Interfaces*, 2014, **6**, 9711-9718.
37. J. Shi, J. Dong, S. Lv, Y. Xu, L. Zhu, J. Xiao, X. Xu, H. Wu, D. Li, Y. Luo and Q. Meng, *Appl. Phys. Lett.*, 2014, **104**, 063901.
38. D. Q. Bi, S. J. Moon, L. Haggman, G. Boschloo, L. Yang, E. M. J. Johansson, M. K. Nazeeruddin, M. Grätzel and A. Hagfeldt, *RSC Adv.*, 2013, **3**, 18762-18766.
39. M. R. Leyden, L. K. Ono, S. R. Raga, Y. Kato, S. Wang and Y. Qi, *J. Mater. Chem. A*, 2014, **2**, 18742-18745.
40. S. Aharon, S. Gamliel, B. E. Cohen and L. Etgar, *Phys. Chem. Chem. Phys.*, 2014, **16**, 10512-10518.
41. A. K. Chandiran, A. Yella, M. T. Mayer, P. Gao, M. K. Nazeeruddin and M. Grätzel, *Adv. Mater.*, 2014, **26**, 4309-4312.
42. K.-G. Lim, H.-B. Kim, J. Jeong, H. Kim, J. Y. Kim and T.-W. Lee, *Adv. Mater.*, 2014, **26**, 6461-6466.
43. T. M. Koh, S. Dharani, H. Li, R. R. Prabhakar, N. Mathews, A. C. Grimsdale and S. G. Mhaisalkar, *ChemSusChem*, 2014, **7**, 1909-1914.
44. J. H. Heo, S. H. Im, J. H. Noh, T. N. Mandal, C.-S. Lim, J. A. Chang, Y. H. Lee, H.-J. Kim, A. Sarkar, M. K. Nazeeruddin, M. Grätzel and S. Il Seok, *Nat. Photon.*, 2013, **7**, 486-491.
45. Q. Chen, H. Zhou, T.-B. Song, S. Luo, Z. Hong, H.-S. Duan, L. Dou, Y. Liu, and Y. Yang, *Nano Lett.*, 2014, **14**, 4158−4163.
46. Y. Zhao, A. M. Nardes and K. Zhu, *Appl. Phys. Lett.*, 2014, **104**, 213906.
47. Q. Wang, Y. Shao, Q. Dong, Z. Xiao, Y. Yuan and J. Huang, *Energy Environ. Sci.*, 2014, **7**, 2359-2365.
48. J. Kim, G. Kim, T. K. Kim, S. Kwon, H. Back, J. Lee, S. H. Lee, H. Kang and K. Lee, *J. Mater. Chem. A*, 2014, **2**, 17291-17296.
49. P. Qin, S. Tanaka, S. Ito, N. Tetreault, K. Manabe, H. Nishino, M. K. Nazeeruddin and M. Grätzel, *Nat. Commun.*, 2014, **5**,3834.
50. L. Gil-Escrig, G. Longo, A. Pertegas, C. Roldan-Carmona, A. Soriano, M. Sessolo and H. J. Bolink, *Chem. Commun.*, 2015, **51**, 569-571.
51. P. Qin, S. Paek, M. I. Dar, N. Pellet, J. Ko, M. Grätzel and M.

K. Nazeeruddin, *J. Am. Chem. Soc.*, 2014, **136**, 8516-8519.
52. W. Chen, Y. Wu, J. Liu, C. Qin, X. Yang, A. Islam, Y.-B. Cheng and L. Han, *Energy Environ. Sci.*, 2015, **8**, 629-640.
53. Y. Wu, A. Islam, X. Yang, C. Qin, J. Liu, K. Zhang, W. Peng and L. Han, *Energy Environ. Sci.*, 2014, **7**, 2934-2938.
54. H. Choi, S. Paek, N. Lim, Y. H. Lee, M. K. Nazeeruddin and J. Ko, Chem. Eur. J., 2014, 20, 10894-10899.
55. A. Yella, L.-P. Heiniger, P. Gao, M. K. Nazeeruddin and M. Grätzel, *Nano Lett.*, 2014, **14**, 2591-2596.
56. J. Seo, S. Park, Y. C. Kim, N. J. Jeon, J. H. Noh, S. C. Yoon and S. Il Seok, *Energy Environ. Sci.*, 2014, **7**, 2642-2646.
57. Q. Hu, J. Wu, C. Jiang, T. Liu, X. Que, R. Zhu and Q. Gong, *ACS Nano*, 2014, **8**, 10161-10167.
58. J. H. Kim, P.-W. Liang, S. T. Williams, N. Cho, C.-C. Chueh, M. S. Glaz, D. S. Ginger and A. K.-Y. Jen, *Adv. Mater.*, 2015, **27**, 695-701.
59. L. Zuo, Z. Gu, T. Ye, W. Fu, G. Wu, H. Li and H. Chen, *J. Am. Chem. Soc.*, 2015, **137**, 2674-2679.
60. D. Liu and T. L. Kelly, *Nat. Photon.*, 2013, **8**, 133-138.
61. A. Abate, M. Saliba, D. J. Hollman, S. D. Stranks, K. Wojciechowski, R. Avolio, G. Grancini, A. Petrozza and H. J. Snaith, *Nano Lett.*, 2014, **14**, 3247-3254.
62. F. Huang, Y. Dkhissi, W. Huang, M. Xiao, I. Benesperi, S. Rubanov, Y. Zhu, X. Lin, L. Jiang, Y. Zhou, A. Gray-Weale, J. Etheridge, C. R. McNeill, R. A. Caruso, U. Bach, L. Spiccia and Y.-B. Cheng, *Nano Energy*, 2014, **10**, 10-18.
63. J.-H. Im, I.-H. Jang, N. Pellet, M. Grätzel and N.-G. Park, *Nat. Nanotechnol.*, 2014, **9**, 927-932.
64. J. H. Heo, H. J. Han, D. Kim, T. K. Ahn and S. H. Im, *Energy Environ. Sci.*, 2015, **8**, 1602-1608.
65. K. W. Tan, D. T. Moore, M. Saliba, H. Sai, L. A. Estroff, T. Hanrath, H. J. Snaith and U. Wiesner, *ACS Nano*, 2014, **8**, 4730-4739.
66. P. Docampo, J. M. Ball, M. Darwich, G. E. Eperon and H. J. Snaith, *Nat. Commun.*, 2013, **4**, 2761.
67. B. Conings, L. Baeten, C. D. Dobbelaere, J. D'Haen, J. Manca and H.-G. Boyen, *Adv. Mater.*, 2014, **26**, 2041-2046.
68. J. You, Z. Hong, Y. M. Yang, Q. Chen, M. Cai, T. B. Song, C. C.Chen, S. Lu, Y. Liu, H. Zhou and Y. Yang, *ACS Nano*, 2014, **8**, 1674-1680.
69. D. Wang, Z. Liu, Z. Zhou, H. Zhu, Y. Zhou, C. Huang, Z. Wang, H. Xu, Y. Jin, B. Fan, S. Pang, and G. Cui, *Chem. Mater.*, 2014, **26**, 7145-7150.
70. A. Abrusci, S. D. Stranks, P. Docampo, H. L. Yip, A. K. Jen and H. J. Snaith, *Nano Lett.*, 2013, **13**, 3124-3128.
71. J. M. Ball, M. M. Lee, A. Hey and H. J. Snaith, *Energy Environ. Sci.*, 2013, **6**, 1739-1743.
72. D. Sabba, A. D. Herlina, R. P. Rajiv, B. Tom, S.Chen, Y. Du, M. Nripan, P. B. Pablo and G. M. Subodh, *Nanoscale*, 2014, **6**, 13854-13860.
73. Q. Xue, Z. Hu, J. Liu, J. Lin, C. Sun, Z. Chen, C. Duan, J. Wang, C. Liao, W. M. Lau, F. Huang, H.-L. Yip and Y. Cao, *J. Mater. Chem. A*, 2014, **2**, 19598-19603.
74. W. Zhang, M. Saliba, D. T. Moore, S. K. Pathak, M. T. Horantner, T. Stergiopoulos, S. D. Stranks, G. E. Eperon, J. A. Alexander-Webber, A. Abate, A. Sadhanala, S. Yao, Y. Chen, R. H. Friend, L. A. Estroff, U. Wiesner and H. J. Snaith, *Nat. Commun.*, 2015, **6**, 6142-6151.
75. N. K. Noel, A. Abate, S. D. Stranks, E. S. Parrott, V. M. Burlakov, A. Goriely and H. J. Snaith, *ACS Nano*, 2014, **8**, 9815-9821.
76. C.-W. Chen, H.-W. Kang, S.-Y. Hsiao, P.-F. Yang, K.-M. Chiang and H.-W. Lin, *Adv. Mater.*, 2014, **26**, 6647-6652.
77. J. T. Wang, J. M. Ball, E. M. Barea, A. Abate, J. A. Alexander-Webber, J. Huang, M. Saliba, I. Mora-Sero, J. Bisquert, H. J. Snaith and R. J. Nicholas, *Nano Lett.*, 2014, **14**, 724-730.
78. K. Wojciechowski, M. Saliba, T. Leijtens, A. Abate and H. J. Snaith, *Energy Environ. Sci.*, 2014, **7**, 1142-1147.
79. Y. Li, J. K. Cooper, R. Buonsanti, C. Giannini, Y. Liu, F. M. Toma and I. D. Sharp, *J. Phys. Chem. Lett.*, 2015, **6**, 493-499.
80. K. Wojciechowski, S. D. Stranks, A. Abate, G. Sadoughi, A. Sadhanala, N. Kopidakis, G. Rumbles, C.-Z. Li, R. H. Friend, A. K.-Y. Jen and H. J. Snaith, *ACS Nano*, 2014, **8**, 12701-12709.
81. W. Nie, H. Tsai, R. Asadpour, J.-C. Blancon, A. J. eukirch, G. Gupta, J. J. Crochet, M. Chhowalla, S. Tretiak, M. A. Alam, S.-L. Wang and A. D. Mohite, *Science*, 2015, **347**, 522-525.
82. H. Zhou, Q. Chen, G. Li, S. Luo, T.-B. Song, H.-S. Duan, Z. Hong, J. You, Y. Liu and Y. Yang, *Science*, 2014, **345**, 542-546.
83. E. Edri, S. Kirmayer, D. Cahen and G. Hodes, *J. Phys. Chem. Lett.*, 2013, **4**, 897-902.
84. B. Cai, Y. D. Xing, Z. Yang, W. H. Zhang and J. S. Qiu, *Energy Environ. Sci.*, 2013, **6**, 1480-1485.
85. J. H. Noh, S. H. Im, J. H. Heo, T. N. Mandal and S. Il Seok, *Nano Lett.*, 2013, **13**, 1764-1769.
86. S. Ryu, J. H. Noh, N. J. Jeon, Y. C. Kim, W. S. Yang, J. Seoa and S. Il Seok, *Energy Environ. Sci.*, 2014, **7**, 2614-2618.
87. J. H. Heo, D. H. Song and S. H. Im, *Adv. Mater.*, 2014, **26**, 8179-8183.
88. S. Aharon, B. E. Cohen and L. Etgar, *J. Phys. Chem. C*, 2014, **118**, 17160-17165.
89. N. J. Jeon, J. H. Noh, Y. C. Kim, W. S. Yang, S. Ryu and S. Il Seok, *Nat. Mater.*, 2014, **13**, 897-903.
90. E. Edri, S. Kirmayer, M. Kulbak, G. Hodes and D. Cahen, *J. Phys. Chem. Lett.*, 2014, **5**, 429-433.
91. Y. Tidhar, E. Edri, H. Weissman, D. Zohar, G. Hodes, D. Cahen, B. Rybtchinski and S. Kirmayer, *J. Am. Chem. Soc.*, 2014, **136**, 13249-13256.
92. S. Pang, H. Hu, J. Zhang, S. Lv, Y. Yu, F. Wei, T. Qin, H. Xu, Z. Liu and G. Cui, *Chem. Mater.*, 2014, **26**, 1485-1491
93. G. E. Eperon, S. D. Stranks, C. Menelaou, M. B. Johnston, L. M. Herz and H. J. Snaith, *Energy Environ. Sci.*, 2014, **7**, 982-988.
94. J.-W. Lee, D.-J. Seol, A.-N. Cho and N.-G. Park, *Adv. Mater.*, 2014, **26**, 4991-4998
95. S. Lv, S. Pang, Y. Zhou, N. P. Padture, H. Hu, L. Wang, X. Zhou, H. Zhu, L. Zhang, C. Huang and G. Cui, *Phys. Chem. Chem. Phys.*, 2014, **16**, 19206-19211.
96. W. S. Yang, J. H. Noh, N. J. Jeon, Y. C. Kim, S. Ryu, J. Seo and S. Il Seok, *Science*, 2015, DOI: science.aaa9272.
97. F. C. Hanusch, E. Wiesenmayer, E. Mankel, A. Binek, P. Angloher, C. Fraunhofer, N. Giesbrecht, J. M. Feckl, W.

Jaegermann, D. Johrendt, T. Bein and P. Docampo, *J. Phys. Chem. Lett.*, 2014, **5**, 2791.

98. F. C. Hanusch, E. Wiesenmayer, E. Mankel, A. Binek, P. Angloher, C. Fraunhofer, N. Giesbrecht, J. M. Feckl, W. Jaegermann, D. Johrendt, T. Bein and P. Docampo, *J. Phys. Chem. Lett.*, 2014, **5**, 2791–2795.
99. N. Pellet, P. Gao, G. Gregori, T. Y. Yang, M. K. Nazeeruddin, J. Maier and M. Grätzel, *Angew. Chem. Int. Ed.*, 2014, **53**, 3151-3157.
100. F. Hao, C. C. Stoumpos, D. H. Cao, R. P. H. Chang and M. G. Kanatzidis, *Nat. Photon.*, 2014, **8**, 489-494.
101. Y. Ogomi, A. Morita, S. Tsukamoto, T. Saitho, N. Fujikawa, Q.Shen, T. Toyoda, K. Yoshino, S. S. Pandey, T. Ma and S.Hayase, *J. Phys. Chem. Lett.*, 2014, **5**, 1004-1011.
102. F. Zuo, S. T. Williams, P.-W. Liang, C.-C. Chueh, C.-Y. Liao and A. K.-Y. Jen, *Adv. Mater.*, 2014, **26**, 6454-6460.
103. Y. Shao, Z. Xiao, C. Bi, Y. Yuan, J. Huang, *Nat. Commun.*, 2014, doi: 10.1038/ncomms6784 .
104. J.-Y. Jeng, K.-C. Chen, T.-Y. Chiang, P.-Y. Lin, T.-D. Tsai, Y.-C. Chang, T.-F. Guo, P. Chen, T.-C. Wen and Y.-J. Hsu, *Adv. Mater.*, 2014, **26**, 4107-4113.
105. J. Cui, F. Meng, H. Zhang, K. Cao, H. Yuan, Y. Cheng, F. Huang and M. Wang, *ACS Appl. Mater. Interfaces*, 2014, **6**, 22862-22870.
106. H. Azimi, T. Ameri, H. Zhang, Y. Hou, C. O. R. Quiroz, J. Min, M. Hu, Z.-G. Zhang, T. Przybilla, G. J. Matt, E. Spiecker, Y. Li and C. J. Brabec, *Adv. Energy Mater.*, 2015, 1401692.
107. P.–W. Liang, C.–Y. Liao, C.–C. Chueh, F. Zuo, S. T. Williams, X.-K. Xin, J. Lin and A. K.-Y. Jen, *Adv. Mater.*, 2014, **26**, 3748–3754.
108. Y. Ogomi, A. Morita, S. Tsukamoto, T. Saitho, Q. Shen and T. Toyoda, *J. Phys. Chem. C*, 2014, **118**, 16651-16659.
109. B. Suarez, V. Gonzalez-Pedro, T. S. Ripolles, R. S. Sanchez, L. Otero and I. Mora-Sero, *J. Phys. Chem. Lett.*, 2014, **5**, 1628-1635.
110. L. Liu, A. Mei, T. Liu, P. Jiang, Y. Sheng, L. Zhang and H. Han, *J. Am. Chem. Soc.*, 2015, **137**, 1790−1793.
111. G. S. Han, H. S. Chung, B. J. Kim, D. H. Kim, J. W. Lee, B. S. Swain, K. Mahmood, J. S. Yoo, N.-G. Park, J. H. Lee and H. S. Jung, *J. Mater. Chem. A*, 2015, **3**, 9160-9164.
112. P. Qin, A. L. Domanski, A. K. Chandiran, R. Berger, H. Butt, M. I. Dar, T. Moehl, N. Tétreault, P. Gao, S. Ahmad, N. Mohammad K. and M. Grätzel, *Nanoscale*, 2014, **6**, 1508-1514.
113. J. Zhang, Z. Hu, L. Huang, G. Yue, J. Liu, X. Lu, Z. Hu, M. Shang, L. Han and Y. Zhu, *Chem. Commun.*, 2015, **51**, 7047-7050.
114. Y. Xu, J. Shi, S. Lv, L. Zhu, J. Dong, H. Wu, Y. Xiao, Y. Luo, S. Wang, D. Li, X. Li and Q. Meng, *ACS Appl. Mater. Interfaces*, 2014, **6**, 5651-5656.
115. J. Shi, X. Xu, D. Li and Q. Meng, *Small*, 2015, DOI: 10.1002/smll.201403534.
116. W. Feng, S. Rangan, Y. Cao, E. Galoppini, R. A. Bartynskib and E. Garfunkel, *J. Mater. Chem. A*, 2014, **2**, 7034-7044.
117. M. C. Scharber, D. Muhlbacher, M. Koppe, P. Denk, C. Waldauf, Alan J. Heeger and C. J. Brabec, *Adv. Mater.*, 2006, *18*, 789-794.
118. P. Schulz, E. Edri, S. Kirmayer, G. Hodes, D. Cahen and A. Kahn, *Energy Environ. Sci.*, 2014, **7**,1377-1381.
119. B. Peng, G. Jungmann, C. Jäger, D. Haarer, H. Schmidt and M. Thelakkat, *Coord. Chem. Rev.*, 2004, **248**, 1479-1489.
120. N.–G. Park**,** *J. Phys. Chem. Lett.*, 2013, **4**, 2423–2429.
121. P. Schulz, L. L. Whittaker-Brooks, B. A. MacLeod, D. C. Olson, Y.-L. Loo and A. Kahn, *Adv. Mater. Interfaces*, 2015, 1400532.
122. T. Yajima, Y. Hikita, M. Minohara, C. Bell, J. A. Mundy, L. F. Kourkoutis, D. A. Muller, H. Kumigashira, M. Oshima and H. Y. Hwang, *Nat. Commun.*, 2015, **6**, 6759.
123. Q. Shen, Y. Ogomi, J. Chang, S. Tsukamoto, K. Kukihara, T. Oshima, N. Osada, K. Yoshino, K. Katayama, T. Toyoda and S. Hayase, *Phys. Chem. Chem. Phys.*, 2014, **16**, 19984-19992.
124. A. Dualeh, T. Moehl, N. Tetreault, J. Teuscher, P. Gao, M. K. Nazeeruddin and M. Grätzel, *ACS Nano*, 2013, **8**, 362-373.
125. E. J. Juarez-Perez, M. Wubler, F. Fabregat-Santiago, K. Lakus-Wollny, E. Mankel, T. Mayer, W. Jaegermann and I. Mora-Sero, *J. Phys. Chem. Lett.*, 2014, **5**, 680-685.
126. K.-S. Liao, S. D. Yambem, A. Haldar, N. J. Alley and S. A. Curran, *Energies*, 2010, **3**, 1212-1250.
127. C. J. Brabec, S. E. Shaheen, C. Winder, N. S. Sariciftci and P. Denk, *Appl. Phys. Lett.*, 2002, **80**, 1288-1290.
128. Z. He, C. Zhong, S. Su, M. Xu, H. Wu and Y. Cao, *Nat. Photon.*, 2012, **6**, 591-595.
129. C. Duan, W. Cai, B. B. Hsu, C. Zhong, K. Zhang, C. Liu, Z. Hu, F. Huang, G. C. Bazan and A. J. Heeger, *Energy Environ. Sci.*, 2013, **6**, 3022-3034.
130. J. Min, Z.-G. Zhang, Y. Hou, C. O. R. Quiroz, T. Przybilla, C. Bronnbauer, F. Guo, K. Forberich, H. Azimi, T. Ameri, E. Spiecker, Y. Li and C. J. Brabec, *Chem. Mater.*, 2015, **27**, 227-234.
131. P. Peumans and S. R. Forrest, *Appl. Phys. Lett.*, 2001, **79**, 126-128.
132. P. Peumans, A. Yakimov and S. R. Forrest, *J. Appl. Phys.*, 2003, **93**, 3693-3723.
133. F. W. Guo, B. Yang, Y. B. Yuan, Z. G. Xiao, Q. F. Dong, Y. Bi and J. S. Huang, *Nat. Nanotechnol.*, 2012, **7**, 798-802.
134. H. J. Snaith and M. Grätzel, *Adv. Mater.*, 2006, **18**, 1910-1914.
135. F. Brivio, A. B. Walker and A. Walsh, *Apl. Mater.*, 2014, **2**, 081506.
136. X. Wu, M. T. Trinh, D. Niesner, H. Zhu, Z. Norman, J. S. Owen, O. Yaffe, B. J. Kudisch and X.-Y. Zhu, *J. Am. Chem. Soc.*, 2015, **137**, 2089-2096.
137. H. Kusano, S. Hosaka, N. Shiraishi, S. Kawakami, K. Sugioka, M. Kitagawa, K. Ichino and H. Kobayashi, *Synth. Met.*, 1997, **91**, 337-339.
138. X. Li, M. Tschumi, H. Han, S. S. Babkair, R. A. Alzubaydi, A. A. Ansari, S. S. Habib, M. K. Nazeeruddin, S. M. Zakeeruddin and M. Grätzel, *Energy Technol.*, 2015, **3**, 1-5.
139. D. Bi, L. Yang, G. Boschloo, A. Hagfeldt and E. M. J. Johansson, *J. Phys. Chem. Lett.*, 2013, **4**, 1532-1536.
140. A. K. Jena, H.-W. Chen, A. Kogo, Y. Sanehira, M. Ikegami and T. Miyasaka, *ACS Appl. Mater. Interfaces*, 2015, **7**, 9817-9823.

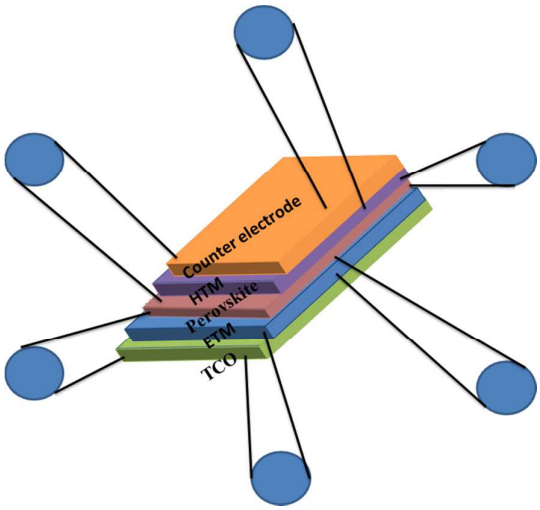

Possible interfaces in a perovskite solar cell

In this review, we present the recent advances about interface engineering at different interfaces in perovskite solar cells.